Available online at www.sciencedirect.com
SCIENCE DIRECT®
Journal of Catalysis 222 (2004) 439–449
JOURNAL OF CATALYSIS
www.elsevier.com/locate/jcat

Adsorption of activated ketones on platinum and their reactivity to hydrogenation: a DFT study

Angelo Vargas, Thomas Bürgi [1], and Alfons Baiker *

Institute for Chemical and Bioengineering, Swiss Federal Institute of Technology, ETH-Hönggerberg, CH-8093 Zurich, Switzerland

Received 14 October 2003; accepted 12 December 2003

Abstract

The adsorption of several ketones interesting for the enantioselective hydrogenation on cinchona-modified platinum has been modeled using relativistically corrected density functional theory. Two metal clusters, containing 19 and 31 Pt atoms, respectively, have been used to model a Pt(111) surface. The two adsorption modes η^1 and η^2 have been described, and their importance for the mechanism of hydrogenation has been pointed out. The effect of an ester group in α position and of α-fluorination of a ketone on its adsorption has been studied, and an explanation for the reactivity enhancement due to the ketone substitution has been proposed.

Keywords: Ketones; Adsorption; Platinum; Hydrogenation; DFT

1. Introduction

The enantioselective hydrogenation of α-keto esters on cinchona-modified platinum [1–6] is, together with the hydrogenation of β-keto esters on tartrate-modified nickel [7], the most thoroughly studied enantioselective hydrogenation in the field of heterogenous catalysis. The inherent technical advantages of heterogeneous catalysis with regard to separation, regeneration, reuse, and handling of the catalyst, together with the steadily growing demand for enantiopure compounds, explain the interest in this catalytic approach and the attempt to extend its scope [8–13]. It has been noted that α-keto esters are "activated" compounds, in the sense that the reactivity of the carbonyl group in various reactions, including the racemic hydrogenation, is greatly enhanced compared to that of other unsubstituted ketones. Other activated compounds have been identified in the class of α-trifluoro-substituted ketones [14,15]. The activation was first associated with the electron-withdrawing capacity of the substituent on the keto carbonyl moiety [14], but also the electronic structure at the HOMO–LUMO orbital level has been cited to explain the different reaction rates in the racemic hydrogenation of a series of substituted acetophenones [16,17]. Also the well-known phenomenon of the rate acceleration due to the surface modifier, the cinchona alkaloid, in the case of the hydrogenation of ethyl pyruvate, could be rationalized within this model [16,17]. All the substrates that gave good enantioselectivity when hydrogenated on a Pt/cinchona catalyst were activated; that is, their hydrogenation on platinum was fast also in the absence of cinchona alkaloids. Furthermore, a slow racemic hydrogenation increases the probability of undesired side reactions such as surface decomposition or loss of regioselectivity. Racemic reaction rate thus becomes a critical point in the search for substrates suitable for enantioselective hydrogenation. Despite the correlations established between the hydrogenation rate of keto groups and properties of the free reactant itself, the mechanism of activation is not well understood, due to the lack of information on the molecular scale. Clearly for a heterogeneously catalyzed reaction "activation" can have a different origin, related on the one hand to the stability of the adsorbed precursor and on the other hand to the transition state.

In this work we will mainly address the adsorption of ketones on a platinum surface, by modeling the Pt(111) surface with a cluster of platinum atoms, and by studying the structural changes that the ketones undergo when interacting with the metal. The focus is set on the determination of the role of the surface in the creation of activated sur-

* Corresponding author.
E-mail address: baiker@tech.chem.ethz (A. Baiker).
[1] *Present address:* Institut de Chimie, Université de Neuchâtel, Switzerland.

0021-9517/$ – see front matter
doi:10.1016/j.jcat.2003.12.006

face intermediates versus spectator species, and on how this may influence the reactivity of the substrates. As model system acetone has been studied and compared to trifluoroacetone, in order to understand the role of α-trifluorination in enhancing reactivity. Methyl pyruvate has been studied in order to understand the role of the ester group in the α position for the hydrogenation reaction. Also the acetophenone–trifluoroacetophenone couple has been compared concerning the formation of activated intermediates on the surface. Based on the findings two different mechanisms for the origin of activation in racemic hydrogenation are proposed.

2. Computational methods

All the cluster calculation have been performed using the Amsterdam Density Functional (ADF) program package [18]. A frozen core approximation was used for the inner core of all the atoms. The 1s orbitals were kept frozen for all second row elements, while orbitals up to 4f were kept frozen for platinum. Decreasing the Pt frozen core to 4d, which implies the explicit calculation of 14 additional electrons per platinum atom, has been shown to increase the adsorption energy of benzene by only about 5 kJ/mol [19]. The importance of relativistic effects has been shown for calculations of platinum [20,21]. The core was modeled using a relativistically corrected pseudopotential created with the DIRAC utility in the ADF program. The DIRAC calculations imply the local density functional in its simple X-alpha approximation without any gradient corrections, but the fully relativistic Hamiltonian is used, including spin-orbit coupling. It was shown that the scalar relativistic correction could account for up to 70% of the total energy in the adsorption of carbon monoxide on platinum, and that also the calculated adsorption site was influenced by the use of a relativistic correction [20]. The relativistic scalar approximation (mass-velocity and Darwin corrections) was therefore used for the Hamiltonian, with the zero order regular approximation (ZORA) method [22], where spin-orbit coupling is included already in zero order. The first-order Pauli formalism [23] was shown to have theoretical deficiencies due to the behavior of the Pauli Hamiltonian at the nucleus, which lead to variational collapse [24] for increasing basis set size. The ZORA formalism requires a special basis set, including much steeper core-like functions, that are implemented in the code. Within this basis set the double-ζ (DZ), double-ζ + polarization (DZP), and triple-ζ + polarization (TZP) basis functions were used for elements of the second period, while the double-ζ basis set was always used for Pt. The local part of the exchange and correlation functional was modeled using a Vosko et al. [25] parametrization of the electron gas. The nonlocal part of the functional was modeled using the Becke correction [26] for the exchange and the Perdew correction [27] for the correlation. Two metal clusters were used: a 19 platinum atoms cluster and a 31 platinum atoms cluster, as shown in Fig. 1. The large 31 atoms cluster was used for the adsorption of the larger molecules such as acetophenone, in order to avoid edge effects. Adsorption energies were calculated as follows:

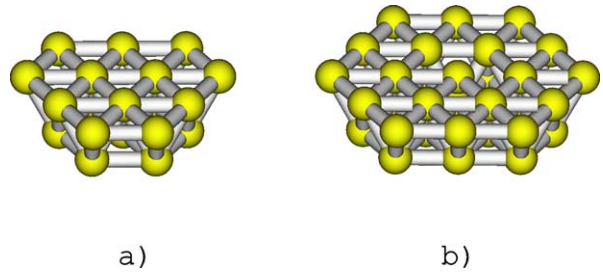

Fig. 1. Pt 19 (a) and Pt 31 (b) clusters used for the adsorption of the ketones.

$$\Delta E_{\text{ads}} = E_{\text{cluster+adsorbate}} - E_{\text{cluster}} - E_{\text{free molecule}},$$

where $E_{\text{cluster+adsorbate}}$ was the energy of the cluster with the molecule adsorbed, E_{cluster} was the energy of the isolated cluster, and $E_{\text{free molecule}}$ was the energy of the free molecule.

Both the Pt 19 and the Pt 31 clusters were spin-optimized, in order to find the spin state with the lowest energy. The Pt 19 cluster was found to have optimal spin state α–$\beta = 6$, while the most stable spin state for the Pt 31 cluster was found to be α–$\beta = 8$, where α–β indicates the difference between α and β electrons, as used in the ADF code. Both clusters were then used with their optimized spin state for the adsorption studies. The semihydrogenated species adsorbed on the Pt 19 clusters were calculated with spin α–$\beta = 5$, therefore considering the adsorbed semihydrogenated molecule as a radical species. The mixing coefficient was also tested, for the Pt 19 and the Pt 31 clusters, by trying a series of values for all the spin states from α–$\beta = 0$ to 10, but the default value of 0.02 was found to be the most efficient for convergence. The latter was nevertheless slow, as expected for these systems, requiring typically more than 100 SCF cycles. All calculations were run unrestricted. The bond distance for the platinum was fixed to the experimental value of 2.775 Å for bulk Pt metal [28]. Molden [29] was used as graphical interface.

3. Results and discussion

3.1. The adsorption of acetone and trifluoroacetone on platinum

The comparison between the adsorption of acetone (AC) and trifluoroacetone (TFAC) should help to understand the effect that the trifluoromethyl substitution has on the keto-carbonyl group. AC is the simplest ketone and shows activation to hydrogenation by platinum when trifluorinated. Experiments show that acetone is hydrogenated very slowly on platinum, while TFAC reacts faster. Under standard reaction conditions [30] the conversion of acetone during racemic hydrogenation was 59% after 2 h, while in the presence of

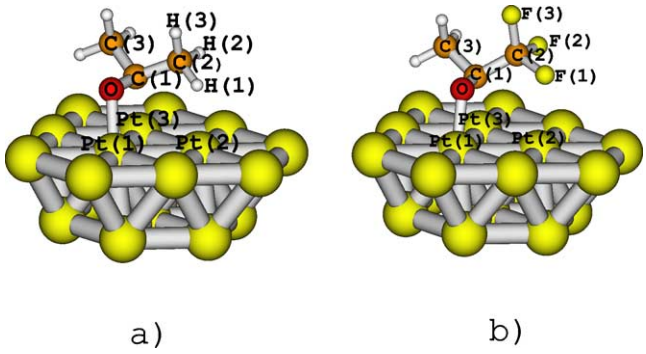

Fig. 2. η^2 adsorption of acetone (a) and trifluoroacetone (b) on Pt 19 cluster.

Table 1
Adsorption energies (kcal/mol), bond lengths (Å), and angles (degrees) for the η^2-adsorbed acetone (AC) and trifuoroacetone (TFAC), with the DZ and DZP basis sets, and with the DZP basis set and selected free platinum atoms

	DZ		DZP		DZP-free	
	AC	TFAC	AC	TFAC	AC	TFAC
Ads. energy	6.8	13.1	−0.8	−0.1	7.1	8.0
C(1)–O	1.43	1.43	1.33	1.35	1.35	1.36
C(1)–C(2)	1.53	1.54	1.52	1.56	1.52	1.55
C(1)–C(3)	1.53	1.54	1.52	1.53	1.52	1.53
C(3)–C(1)–O–C(2)	125°	118°	132°	121°	130°	122°
C(2)–F(1)		1.43		1.35		1.36
C(2)–F(2)		1.43		1.36		1.36
C(2)–F(3)		1.44		1.37		1.37
C(2)–H(1)	1.12		1.12		1.12	
C(2)–H(2)	1.10		1.10		1.10	
C(2)–H(3)	1.11		1.11		1.11	
Pt(1)–O	2.12	2.12	2.16	2.18	2.12	2.10
Pt(2)–H(1)	2.21		2.17		2.24	
Pt(2)–F(1)	2.21	2.59		3.06		2.78
Pt(3)–C(1)	2.21	2.21	2.34	2.24	2.22	2.17

The adsorption geometry is as shown in Fig. 2.

cinchonidine (CD) the conversion was only 13%. The conversion of trifluoroacetone in racemic hydrogenation was complete after 90 min, while in the presence of CD it was complete after 25 min. The e.e. in this case was 19% [31]. The adsorption of acetone on transition metals has been studied by EELS [32] and two different adsorption modes were identified: a η^1 mode (or End-On), found on Pt, adsorbed via the oxygen, and a η^2 mode (or Side-On), found on Ru, adsorbed via the keto carbonyl Π system. The latter was identified as a stable intermediate in the decomposition of acetone. The η^2-adsorbed AC was found to have undergone a rehybridization to nearly sp^3, and to possess a carbonyl bond elongated by approximately 0.1 Å. These two species were considered by the authors to be fundamentally different. Fig. 2 shows the calculated η^2 adsorptions of AC and TFAC on Pt, and Table 1 gives the bond angles and adsorption energies for this interaction mode. The adsorption energies are slightly larger for the fluorinated molecule than for the non fluorinated one.

To partially account for the relaxation of the surface due to chemisorption, a calculation was also performed where

Table 2
Bond lengths (Å) and angles (degrees) for the free acetone (AC), 2-propanol (2PRO), trifluoroacetophenone (TFAC), and 1,1,1-trifluoro-2-propanol (T2PRO), with the DZ and DZP basis sets

	DZ				DZP			
	AC	2PRO	TFAC	T2PRO	AC	2PRO	TFAC	T2PRO
C(1)–O	1.26	1.50	1.24	1.47	1.22	1.44	1.21	1.42
C(1)–C(2)	1.51	1.53	1.56	1.52	1.51	1.52	1.56	1.52
C(3)–C(1)–O–C(2)		126°		125°		126°		125°
C(2)–F(1)			1.41	1.42			1.34	1.36
C(2)–F(2)			1.43	1.43			1.37	1.36
O(1)–H		1.00		1.00		0.98		0.98

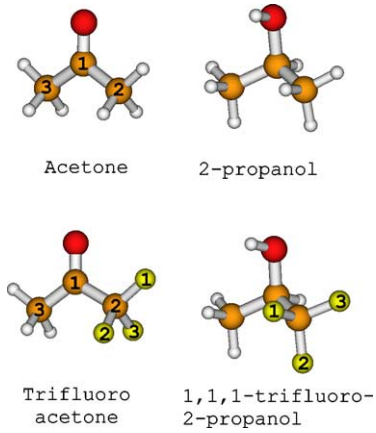

Fig. 3. Free acetone, trifluoroacetone, and the derived alcohols.

the three central platinum atoms of the Pt 19 cluster (Pt(1), Pt(2), and Pt(3) in Fig. 2) were set free to optimize their positions and relax. Entry DZP-free in Table 1 refers to such calculations.

As already reported by Saeys et al. [19] the surface relaxation leads to an increase of the adsorption energy, that in this case amounts to 7–8 kcal/mol. The free platinum atoms increase their distance from the lower layer of the cluster. DZP basis set without relaxation of the central platinum atoms shows slightly negative values of adsorption energy, that increase again after relaxing the cluster. The geometrical parameters for η^2 adsorbed and free AC and TFAC are listed in Tables 1 and 2, respectively. In the η^2 adsorption mode the keto-carbonyl bond length is remarkably stretched to a bond length that is half way between that of the ketones and that of the hydrogenation products, 2-propanol (2PRO) and 1,1,1-trifluoro-2-propanol (T2PRO). The values with a DZP basis set are 1.21–1.22 Å for the free carbonyl (Table 2), 1.35–1.36 Å for the η^2 adsorbed molecule (Table 1), and 1.42–1.44 Å for the C–O of the alcohols (Fig. 3, Table 2). The influence of the basis set is evidently relevant for the adsorbed carbonyl bond length but, as will be shown for the adsorption of methyl pyruvate, tends to stabilize at DZP values. The resulting elongation of 0.1 Å for C–O corresponds to the experimental value found for η^2 adsorption of acetone [32]. Also the bond distances between

Table 3
Adsorption energies (kcal/mol) for η^1 adsorption mode of acetone

Ads. mode	AC			TFAC		
	DZ	DZP	DZP-free	DZ	DZP	DZP-free
a	9.9	7.0	10.9	5.6	–	–
b	10.1	7.2	11.4	6.0	3.5	7.1
c	10.1	7.6	11.7	6.3	4.1	7.6

The three geometries in Fig. 4 have three different cluster-edge effects. The experimental heat of adsorption of AC is 11.5 kcal/mol [32].

the metal and the molecule increased with the addition of polarization functions. This effect may also be due to the fact that it was possible to increase only the basis set of the adsorbed molecule but not that of the platinum. A remarkable rehybridization at the carbonyl C took place for η^2 adsorbates, removing the coplanarity of the carbonyl with the skeleton of the acetone by approximately 50°. A similar rehybridization was found when the adsorption of ethylene on palladium was calculated and transition-state calculations showed that this rehybridized state is the active one for the successive hydrogenation step [33,34]. For ketones, in analogy with ethylene, the rehybridization can be viewed as a step toward the formation of hydrogenated species. In fact the value for the angle C(3)–C(1)–O–C(2) in the alcohols is strikingly close to that of the η^2-adsorbed AC and TFAC. This also corresponds to the experimental findings, according to which the rehybridization of the ketonic carbon from sp^2 to nearly sp^3 takes place. For trifluoroacetone the distortion from planarity is larger due to the repulsion of the fluorine atoms with the platinum surface. Hydrogen atoms on the other hand have bonding interactions with the platinum atoms. Referring to Fig. 2b and Table 1, it can be seen that the C(2)–F(1) bond length is slightly shortened compared to C(2)–F(2) and C(2)–F(3), indicating that nonbonding interactions to the surface are present, while referring to Fig. 2a and Table 1 it can be seen that the hydrogen atoms in the same positions behave in the opposite way and C(2)–H(1) is slightly elongated compared to C(2)–H(2) and C(2)–H(3), due to the bonding interacting with the surface. Also, the Pt–H(1) distance is remarkably shorter than the Pt–F(1) distance and therefore fluorine atoms occupy more space due to the larger C–F bond length (1.4 Å) compared to the C–H bond length (1.1 Å) and cause more distortion to the carbonyl.

Both acetone and trifluoroacetone also have a η^1 adsorption mode, shown in Fig. 4. In this case the edge effects were analyzed by studying the energy and geometrical differences between the adsorptions in contact with edging platinum atoms in the cluster. Fig. 4a shows the η^1-adsorbed acetone with two of the methyl hydrogens in contact with edging platinum atoms, indicated by Pt(4) and Pt(5) in the figure. Fig. 4b shows the adsorption mode where the same contact occurs only with one edging platinum atom, Pt(5). Fig. 4c shows the most symmetric η^1 mode, where the acetone is not in contact with edging atoms. Fig. 4d shows a side view of this latter mode. Table 3 gives the adsorption energies for all the cases, for both acetone and trifluoroacetone.

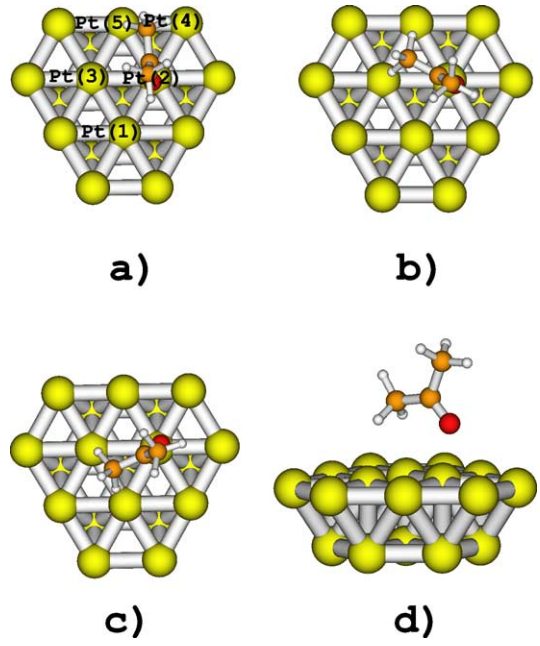

Fig. 4. η^1 adsorption of acetone on Pt 19 cluster. The figure shows the different interactions (a), (b), and (c) of acetone with the same cluster, and a side view (d).

The effect of the edging is to make the interaction less efficient, by a value ranging between 0.1 and 1.0 kcal/mol. The adsorption in Fig. 4a, where two hydrogens are in contact with two edging platinum atoms, is not stable for trifluoroacetone when a DZP basis set is used, and the molecule tends to adjust itself to the interaction shown in Fig. 4b. Evidently the presence of the fluorine atoms makes the bonding of the hydrogen atoms to the metal less efficient. In this interaction mode trifluoroacetone always interacts with the platinum only via the carbonyl oxygen and the methyl hydrogens, while the interaction on the side of the trifluoromethyl group does not occur. In fact when the hydrogens in contact with the surface are replaced by fluorine atoms the molecule is pushed away from the metal, eventually finding either an η^2 adsorption mode or a η^1 mode with hydrogen atoms in contact with the metal. Again the experimental value found for η^1 adsorption of AC is in good agreement with the calculated one at the DZP-free level. It is remarkable that while for acetone the η^1 mode is about 3.0 kcal/mol more stable than the η^2 mode, for trifluoroacetone the two modes are energetically almost equivalent, with a slight preference for the η^2 adsorption. The calculations for AC are in full agreement with experiments which reveal an η^1 adsorption for AC on Pt. The geometries for the three cases in Fig. 4 are almost identical.

Altogether it can be stated that the edges, at least in the case of the contact of a methyl group, do not cause a large bias neither to the structures nor to the adsorption energies. For acetone and trifluoroacetone the η^1 adsorption mode does not show an activation of the carbonyl moiety. The C=O bond lengths of the η^1 adsorbed acetone and trifluoroacetone are very similar to those of the corresponding free

molecules (Table 2). Furthermore for the η^1 mode of adsorption no rehybridization of the double bond is present. Also this result is in agreement with experiments [32].

The most striking difference between fluorinated and nonfluorinated substrates is the different proportion to which we expect the activated intermediate to be present on the surface. Most of the acetone on Pt will be adsorbed as η^1, which is confirmed by the experimental results [32], and act as spectator or precursor species. On the other hand, trifluoroacetone on Pt should have a larger proportion of activated adsorbed intermediate η^2 with respect to η^1. This could be one of the main reasons for its faster catalytic hydrogenation compared to acetone. The difference in adsorption modes found for AC on Pt and Ru has been attributed [32] to the different extent of back-donation of the metal to the π^* orbital of the keto carbonyl moiety. An electron-rich metal with a higher Fermi level is more effective in the interaction with the antibonding states of the molecule's π system, thus enhancing back-donation and favoring the η^2 mode. This explanation fits well to the present findings, as it has already been shown in previous studies [16,17] that the effect of α-fluorination of a ketone is stabilizing both the bonding and the antibonding keto carbonyl π orbitals. Therefore TFAC, with its π^* orbitals stabilized compared to AC, is able to promote η^2 adsorption versus η^1, given the same metal surface.

The cited work by Anton et al. observes that coadsorbed oxygen induces a variation in the relative proportions between η^1 and η^2 species in favor of the η^1, when acetone is adsorbed on Ru(100), and this effect is attributed to the increase in the work function of the metal due to coadsorption of an electronegative atom. In general it is observed by Anton et al. in the cited study that back-bonded species are favored by coadsorbed species, such as the potassium ion, that cause a decrease in work function, while η^1-adsorbed species are favored by the coadsorption of electronegative atoms that increase the work function of the metal. The adsorption of hydrogen on Pt(111) has been shown to decrease the work function of the metal [35], which means that hydrogen coadsorption in a system such as that described in this work would increase the η^2/η^1 ratio. It is therefore inferred that the results presented here are also valid in the presence of coadsorbed hydrogen, only with a further increase in the proportion of η^2-adsorbed species.

The hydrogenation step that follows the η^2 adsorption is believed to occur following a Horiuti–Polanyi mechanism [36] analogous to that described for the hydrogenation of ethylene [33,34]. The detailed description of this step is in course of investigation.

3.2. The adsorption of methyl pyruvate

The enantioselective hydrogenation of ethyl pyruvate (EP) on cinchona-modified platinum [37] has been used as model system for the understanding of the mechanism of enantiodifferentiation. The adsorption of EP has been experimentally studied with different techniques on Ni and Pt

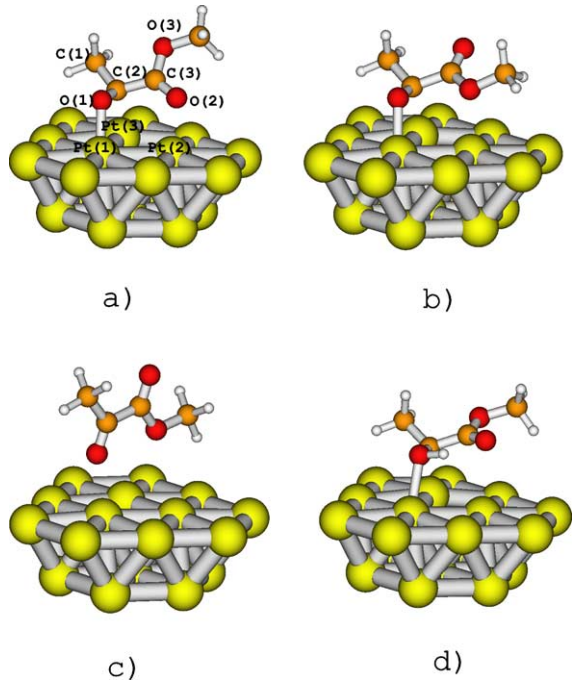

Fig. 5. Adsorption modes of ethyl pyruvate on Pt: (a) η^2-*cis*, (b) η^2-*trans*, (c) η^1-*trans*, and (d) semihydrogenated η^2-*cis*.

[38–41]. While the preferred adsorption of molecular methyl pyruvate (MP) on Ni was found to be a bifurcated version of the η^1 discussed for AC, the studies on Pt point to a mixture of adsorption modes of the ethyl pyruvate. For our studies the use of MP was preferred, because it is lighter than EP, while retaining the same functional groups. Methyl pyruvate has been adsorbed on the Pt 19 cluster both in the *cis* and in the *trans* conformations resulting in the geometries shown in Fig. 5. The *cis* η^2 adsorption (Fig. 2a) resulted the most stable at all levels of theory taken into consideration (Table 4). Only the *trans* conformation showed an energy minimum also in the η^1 adsorption mode shown in Fig. 5c, whereas the *cis* conformer was not stable when η^1 adsorbed. Furthermore the η^1 adsorption mode for the *trans* methyl pyruvate was stable only when the polarization functions were added to the basis set while with the smaller DZ basis set also the *trans* methyl pyruvate tended to lay down on the surface and interact via the keto-carbonyl moiety. The adsorption energies showed a strong bias for η^2 adsorption (Table 4), whereas the η^1 adsorption, avoiding the interaction of the keto-carbonyl carbon with the surface, gave a much weaker interaction. When adsorbed η^2 the main interaction with the metal was given by the keto-carbonyl moiety, which corresponds to the reacting part of the molecule in presence of adsorbed hydrogen. The ester group on the other hand did not interact strongly with the Pt surface once the preferred keto-carbonyl adsorption had taken place. The ester group could not get in contact with the free valence of the platinum atoms, its geometry remaining practically unaltered. The plane identified by the ester group (atoms O(3), C(3), and O(2) in Fig. 5) is not parallel to the metal surface

Table 4
Adsorption energies (kcal/mol), bond lengths (Å), and angles (degrees) for the η^2-adsorbed methyl pyruvate (MP) with the DZ, DZP, and TZP basis sets, and with the DZP and TZP basis sets and relaxation of the three central platinum atoms in the cluster

	DZ		DZP			DZP-free				TZP-free	
	MPC	MPT(1)	MPC	MPT(1)	MPT(2)	MPC	MPT(1)	MPT(2)	SEMI	MPC	MPT(1)
Ads. Energy	23.4	21.3	10.6	6.2	1.2	17.5	14.2	3.0		16.4	10.5
BSSE MP						5.6	6.2			0.9	
BSSE PT						4.4	4.7			6.1	
BSSE TOT						10.0	10.9			7.0	
C(2)–O(1)	1.43	1.43	1.35	1.34	1.22	1.36	1.35	1.22	1.45	1.36	1.35
C(3)–O(2)	1.28	1.24	1.24	1.21	1.22	1.25	1.21	1.22	1.23	1.25	1.21
C(3)–O(3)	1.36	1.43	1.33	1.38	1.34	1.33	1.39	1.33	1.33	1.33	1.39
C(1)–C(2)–O(1)–C(3)	124°	123°	128°	128°	180°	127°	131°	179	122°	130°	128°
C(2)–C(3)–O(3)–C(2)	175°	174°	174°	174°	180°	173°	174°	180°	177°	174°	173°
Pt(1)–O(1)	2.11	2.11	2.12	2.13	2.91	2.10	2.12	2.60	2.32	2.08	2.08
Pt(2)–O(2)	2.22		2.24			2.22			3.00	2.19	
Pt(2)–O(3)		2.29		2.48	3.72		2.45	3.36			2.40
Pt(3)–C(2)	2.20	2.20	2.25	2.26		2.18	2.21		2.12	2.20	2.21
Ester group Tilting	55°	40°	51°	28°		52°	27°			51°	37°

Reference is to Fig. 5.

(Fig. 5), but tilted. The values for this tilting angle are given in the last entry of Table 4.

In short, the methyl pyruvate interacted very strongly through only two of its atoms, and selectively with two platinum atoms of the cluster. Computationally, the effect of the addition of the polarization functions to the DZ basis set (entry DZP in Table 4) was to cause a stronger binding within the carbonyl group of the molecule and a weaker binding of the molecule to the metal cluster atoms.

In order to test the reliability of the Pt 19 cluster, methyl pyruvate was also adsorbed on a Pt 31 cluster (Fig. 1b). The basis set used for carbon, oxygen, and hydrogen was DZ. Adsorption energies for the *cis* and for the *trans* methyl pyruvate resulted in 23.2 and 21.3 kcal/mol, respectively, compared to 23.4 and 21.3 kcal/mol for the Pt 19 cluster calculation with the same basis set (Table 4), indicating that the enlargement of the cluster does not lead to substantial alterations in terms of adsorption energy. Also geometrical parameters remained practically unchanged upon cluster enlargement, thus edge effects can be excluded in this case. The basis set for second row elements was expanded up to TZP (Table 4) and a decrease of adsorption energies was noted, although greater for the *trans* than for the *cis* methyl pyruvate. The overall result was that at the higher level of theory used, the difference in energy between adsorbed *cis* and *trans* methyl pyruvate increased in favor of the *cis* adsorption. Almost 6 kcal/mol of difference should imply a high fractional coverage of the *cis* conformation at equilibrium.

Calculation of the basis set superposition error using the counterpoise method [42] indicated that for the DZP basis set it contributed greatly to the total calculated adsorption energy, as shown in Table 4, but also showed that the BSSE for *cis*- and *trans*-adsorbed species have similar values. Furthermore, when the basis set was expanded to TZP the BSSE decreased dramatically for MP while it remained large for the platinum cluster. DZP was nevertheless the limit size for the basis set used throughout this study because of the size of the system and because the BSSE tends to cancel for energy differences.

Table 5
Bond lengths (Å) and angles (degrees) for the free methyl pyruvate in the *cis* (MPC) and in the *trans* (MPT) conformations, and for the free methyl lactate in the *cis* (MLC) and in the *trans* (MLT) conformations, as shown in Fig. 6, calculated with the DZ and the DZP basis sets

	DZ			DZP			
	MPC	MPT	MLC	MPC	MPT	MLC	MLT
C(2)–O(1)	1.25	1.25	1.47	1.21	1.22	1.42	1.43
C(3)–O(2)	1.24	1.25	1.25	1.21	1.22	1.35	1.21
C(3)–O(3)	1.39	1.38	1.38	1.35	1.34	1.22	1.36
O(1)–H			1.01			0.99	0.98
H–O(2)						2.01	
H–O(3)							2.00
C(1)–C(2)–O(1)–C(3)	180°	180°	123°	180°	180°	122°	124°
C(2)–C(3)–O(3)–C(2)	180°	180°	180°	180°	180°	180°	179°

The bond lengths for selected bonds are listed in Tables 4 and 5, for both the adsorbed methyl pyruvate, in the three geometries shown in Fig. 5, as well as for the free methyl pyruvate, and for methyl lactate. In the η^2 adsorption mode the keto-carbonyl bond length is stretched as already shown for AC. When expanding the basis set for second row elements to TZP (Table 4) the adsorbed keto-carbonyl bond length, and also most other geometrical parameters, remain unaltered, showing that good convergence of the basis set is reached for DZP. The two most visible effects of the basis set increase for second row elements on the geometry are the tighter binding of the oxygens to the metal and the weaker binding through the carbon. Platinum to oxygen bond lengths are slightly shortened and platinum to carbon bonds slightly elongated.

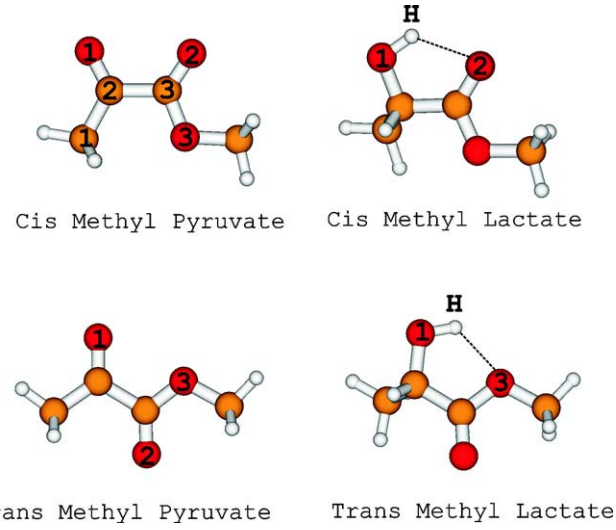

Fig. 6. Free *cis* and *trans* methyl pyruvate and *cis* and *trans* methyl lactate.

Fig. 6 shows that also the methyl lactate (ML) can exist in both a *cis* and a *trans* conformation, according to where the internal hydrogen bond takes place. The energy difference between the two conformers, using a DZP basis set, was of 3.0 kcal/mol, in favor of the *cis* conformer. This difference in energy originates from the more stable intramolecular hydrogen bond between the hydroxylic hydrogen and oxygen 2 rather than oxygen 3. As will be discussed later this may be relevant for the interpretation of the reaction rate of hydrogenation.

The rehybridization of the carbonyl carbon that was already observed for η^2-adsorbed AC, is found also for η^2-adsorbed MP. From a stereochemical point of view, the rehybridization leads to a tridimensionality of the adsorbate and as a consequence the latter becomes chiral, bearing a stereogenic carbon. On the other hand, free methyl pyruvate is only prochiral. This remarkable change in the structure of the adsorbate is due to the direct interaction of the carbon and oxygen of the keto-carbonyl moiety with two atoms of the metal cluster.

The observations described above support the hypothesis that the η^2-adsorbed rehybridized ketone on the platinum surface is an activated species and a reaction intermediate. In the case of MP this stable intermediate is present also on Pt, justifying its high reactivity. This intermediate strongly resembles the alcohol, that is the product of hydrogenation, and therefore, if it is admitted that the adsorption step is not rate determining, is consistent with the hypothesis of a late transition state.

As we have noted above, the *cis* ML, due to the intramolecular hydrogen bond, is more stable than the *trans* conformer. This leads to the further hypothesis that an intramolecular hydrogen bond leads to a lowering of the transition state, and also that this stabilization should be larger for the *cis* than for the *trans* conformer. A semihydrogenated species was therefore calculated, as shown in Fig. 5d, and indeed the α neighboring group strongly interacts with the hydrogen. The presence of the ester group oxygen in other words lowers the energy needed for the hydrogen uptake through hydrogen bonding in the transition state. This may well explain the critical role that an ester group in α position plays in making the hydrogenation of ketones on platinum so efficient. This effect of stabilization of the transition state and the half-hydrogenated species is possible also for other molecules that contain an oxygen atom in the same position. Indeed it has been experimentally observed that molecules such as diketones and α-keto alcohols [43–46] can be catalytically hydrogenated on platinum, as well as α-keto acetals [47,48]. This is further supported by the observation that the hydrogenation of α-keto ethers occurs more efficiently when the conformation of the molecule is fixed in *cis* position in a cyclic molecule rather than when the ether is free to rotate, in which case the activating effect of the oxygen may occur to a lesser extent [49]. The semihydrogenated TFAC was also calculated but in this case no interaction of the added hydrogen with fluorine was observed. It is then strongly suggested that the mechanisms for the activation of α-keto esters just described should not be the same as the one operating for α-trifluorinated species. The effect of fluorine seems to be that of increasing the proportion of η^2-adsorbed ketone, which is the activated species, by destabilizing the η^1 adsorption with respect to the η^2 mode, while an ester in α position is also able to stabilize the transition state and a semihydrogenated intermediate.

Concerning the enantioselectivity of the hydrogenation reaction in the presence of cinchona alkaloids, it is worth noting that the selectivity critically depends on the interaction between the chiral modifier and the adsorbate, resulting in a larger reaction rate to one of the enantiomers either due to thermodynamic or due to kinetic reasons. Intuitively enantiodiscrimination is expected to be larger for a chiral adsorbate as shown in Fig. 5a than for a prochiral molecule.

3.3. The adsorption of acetophenone and trifluoroacetophenone on platinum

Acetophenones have successfully been hydrogenated on cinchona alkaloid-modified platinum. In particular trifluoroacetophenone (TFACPH) has been hydrogenated with high e.e. [14], and many substituted acetophenones have been studied in order to understand the key factors for the activation of the otherwise rather inert acetophenone (ACPH) [17]. ACPH reacts slowly, and the slow formation of the corresponding alcohol makes the hydrogenation of the aromatic ring a competitive reaction. On the other hand, TFACPH reacts almost 10 times faster and shows rate acceleration in the presence of cinchonidine.

For the study of the adsorption of acetophenones, benzene can serve as a reference molecule. Its adsorption on Pt has been calculated before [19,50]. So-called bridge and hollow sites were found to be the most stable (Fig. 7) in good agreement with TPD experiments which revealed two favorite adsorption sites on Pt [51,52]. At high coverage the

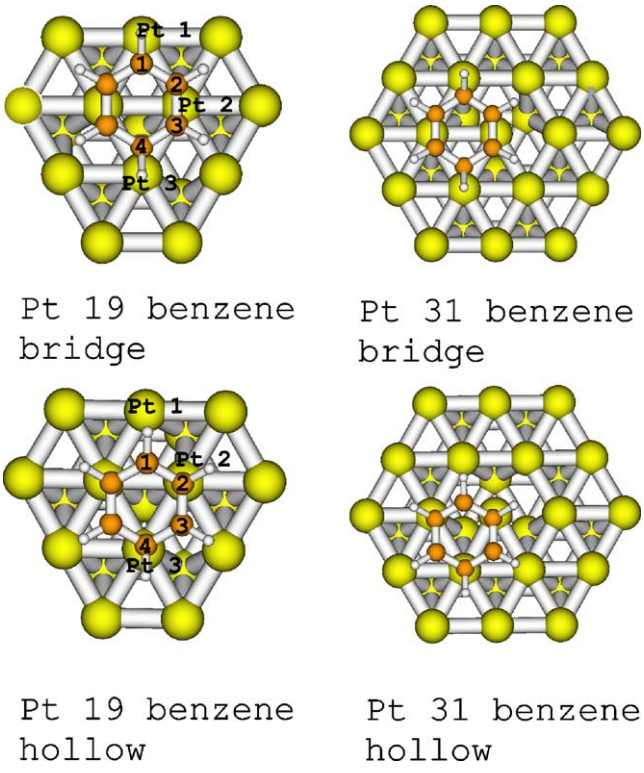

Fig. 7. Adsorption of benzene on Pt 19 and Pt 31 clusters, in both bridge and hollow sites.

Table 6
Adsorption energies (kcal/mol) and bond distances (Å) for the two calculated modes of adsorbed benzene, with the DZ and DZP basis sets, in the hollow and bridge adsorption modes

	Pt 19				Pt 31			
	Bridge		Hollow		Bridge		Hollow	
	DZ	DZP	DZ	DZP	DZ	DZP	DZ	DZP
Ads. energy	16.1	19.2	13.8	12.7	27.8	26.1	15.3	14.2
Pt(1)–C(1)	2.71	2.46	2.97	2.92	2.27	2.27	2.92	2.94
Pt(2)–C(2)	2.53	2.33	2.37	2.35	2.28	2.28	2.35	2.36
Pt(2)–C(3)	2.42	2.28	2.81	2.82	2.26	2.25	2.82	2.81
Pt(3)–C(4)	2.39	2.24	2.37	2.36	2.28	2.29	2.36	2.36
C(1)–C(2)	1.42	1.44	1.43	1.44	1.47	1.46	1.44	1.42
C(2)–C(3)	1.43	1.43	1.43	1.43	1.44	1.43	1.43	1.42
C(3)–C(4)	1.45	1.47	1.43	1.43	1.47	1.46	1.43	1.42

The experimental values for adsorption are 28.0–30.1 kcal/mol for the bridge site and 19.6–20.5 kcal/mol for the hollow site [51,52].

less stable hollow site is more favorable while at low coverage the more stable bridge site takes over. These results were reproduced using our cluster calculations, corroborating that the most stable adsorption site for benzene is the bridge followed by the hollow site.

Table 6 summarizes adsorption geometry parameters and adsorption energy values, with reference to Fig. 7. It should be noted that unlike for methyl pyruvate, where the enlargement of the cluster from Pt 19 to Pt 31 did not induce large variations to both geometry and energy, in the case of benzene the values change remarkably when increasing cluster size. The adsorption on Pt 31 is more stable, and the bond distances from platinum are more uniform compared to those obtained for Pt 19. The bridge site shows values of bond distances from platinum that range from 2.25 to 2.29 Å on Pt 31, evidence of a clearly different behavior from the Pt 19 cluster.

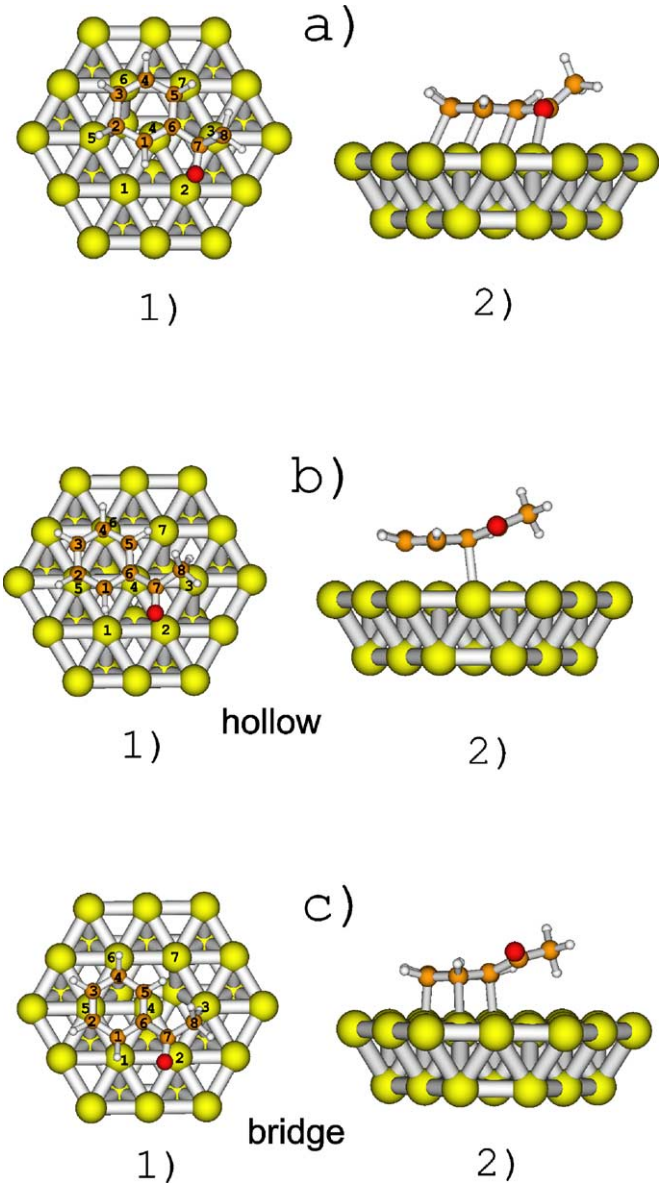

Fig. 8. Adsorption of acetophenone on Pt 31 cluster. 1 and 2 refer to the top and side view, respectively. (a) Adsorption through the carbonyl, (b) adsorption through benzene (hollow), and (c) adsorption through benzene (bridge).

The bridge site also reproduces the experimental values better than the hollow site, for which the calculated adsorption energy is underestimated. Based on the benzene calculation, the DZP basis set with the Pt 31 cluster was judged the best for studying ACPH and TFACPH adsorption, because the edge effects are avoided and the basis set is fairly large. For acetophenones a Pt 19 cluster would have implied

Table 7
Adsorption energies (kcal/mol), bond distances (Å), and angles (degrees) for the three calculated modes of adsorption of acetophenone and trifluoroacetophenone (Fig. 8), respectively, (a) carbonyl adsorption (also η^2), (b) hollow adsorption, and (c) bridge adsorption, with the DZ and DZP basis sets

	ACPH						TFACPH		
	a		b		c		a		c
	DZ	DZP	DZ	DZP	DZ	DZP	DZ	DZP	DZP
Ads. Energy	38.4	27.7	14.9	11.4	25.4	21.6	45.7	30.0	17.5
C(7)–O	1.40	1.33	1.26	1.23	1.27	1.23	1.42	1.34	1.22
C(7)–C(6)	1.52	1.52	1.51	1.51	1.52	1.52	1.53	1.53	1.50
C(8)–C(7)–O–C(6)	135°	140°	177°	176°	170°	176°	128°	128°	164°
Pt(2)–O	2.16	2.19	3.01	3.13	3.35	3.27	2.15	2.15	3.18
Pt(2)–C(7)					3.04	3.09			3.04
Pt(3)–C(7)	2.23	2.30	3.54	3.55			2.19	2.21	
Pt(3)–C(8)	3.12	3.10	3.50	3.40	3.33	3.36	3.14	3.17	3.75
Pt(4)–C(1)	2.20	2.20	2.93	2.92			2.23	2.21	
Pt(1)–C(1)					2.30	2.38			2.27
Pt(4)–C(6)	2.20	2.18	2.45	2.43	2.37	2.42	2.21	2.19	2.37
Pt(4)–C(5)	2.24	2.24	2.92	2.93	2.28	2.32	2.25	2.24	2.27
Pt(7)–C(5)	2.21	2.21	3.11	3.11			2.21	2.21	
Pt(6)–C(4)	2.35	2.32	2.35	2.35	2.28	2.28	2.34	2.32	2.29
C(6)–(5)	1.49	1.48	1.44	1.43	1.45	1.43	1.49	1.48	1.44
C(5)–(4)	1.47	1.46	1.43	1.42	1.47	1.46	1.47	1.46	1.46
C(4)–(3)	1.44	1.42	1.44	1.42	1.47	1.45	1.44	1.43	1.46
C(3)–(2)	1.47	1.46	1.43	1.42	1.44	1.43	1.47	1.46	1.43
C(2)–(1)	1.48	1.46	1.44	1.42	1.47	1.46	1.47	1.46	1.46
C(1)–(6)	1.46	1.45	1.44	1.43	1.47	1.45	1.46	1.45	1.47

Adsorption modes (a), (b), and (c) refer to Fig. 8.

either the keto-carbonyl moiety or the aromatic moiety to be adsorbed on the edges of the cluster.

Fig. 8 shows three adsorption modes of acetophenone: the first one (Fig. 8a) is an adsorption through the keto-carbonyl moiety that shows the features of activation for the keto-carbonyl already observed for calculated AC, TFAC, and MP adsorbed in a η^2 mode. We can therefore due to analogy denote this adsorption mode η^2. The benzene moiety is adsorbed on the surface, but not in one of the optimal modes observed for benzene, i.e., the bridge and hollow adsorptions noted above. The adsorption geometry of the benzene moiety is a hybrid between bridge and hollow, forced by the tight interaction of the carbonyl moiety with the surface. Table 7 gives the values for the adsorption geometry and for the adsorption energy, and it is evident that this interaction mode shows the same features as the interaction modes that we have described above as activated, that is, elongation of the carbonyl C=O bond, rehybridization, and generation of a stereogenic center.

The adsorption mode in Fig. 8b has been obtained by the addition of the keto-carbonyl moiety to the benzene adsorbed in a hollow site as a starting geometry for optimization. This adsorption hinders the direct interaction of the carbonyl with the surface atoms and, as can be clearly seen in Fig. 8b2, favors nonbonding interactions that push away the C=O from the surface. The characteristics that we have identified as activating for the carbonyl are not present in this case. The adsorption in Fig. 8c has been obtained from benzene adsorbed at a bridge site as starting geometry, and analogous considerations can be made as for the adsorption shown in Fig. 8b. Both the bridge and the hollow adsorptions of acetophenone are less stable than the carbonyl adsorption. The greater effectiveness of the η^2 adsorption of acetophenone is also reflected in the longer bond lengths observed for the adsorbed benzene moiety compared to the other two adsorption modes. The bridge adsorption mode shows ring activation through bond elongation to a greater extent than the hollow mode. It is experimentally observed that a part of the acetophenone undergoes ring saturation during enantioselective hydrogenation, and also computationally it is observed that the same adsorption mode that activates the carbonyl also activates the aromatic part of the molecule.

Comparing Tables 6 and 7 we note that benzene is more strongly adsorbed than ACPH, in both bridge and hollow modes. The benzene bond lengths are in the two cases very similar, but the distance from the platinum atoms is larger for ACPH than for benzene. Table 7 also contains the corresponding values obtained for the trifluoroacetophenone. The η^2 adsorption mode is more stable than for acetophenone, and also shows the expected activation parameters, while the hollow adsorption mode is not stable. The simulation shows that the TFACPH moves rather freely on the surface when the geometry optimization starts from a hollow site, without finding an energy minimum. No relevant rehybridization or bond elongation occurs, showing a quasi-physisorbed behavior. The bridge adsorption mode has a smaller adsorption energy than η^2 adsorption, and shows a greater contribution of nonbonding interactions than acetophenone. As noted for TFAC, the fluorine atoms do not have bonding interactions with the surface and have the effect of pushing part of the

molecule away from the surface. This can be seen for example by the bond length Pt(3)–C(8) in Table 7 for the bridge adsorption mode. Also for TFACPH as for TFAC the trifluorination shifts the equilibrium between different adsorption modes toward the η^2. While for ACPH the bridge (nonactivated) adsorption mode has comparable adsorption energy with the η^2 adsorption mode, for the TFACPH the bridge (nonactivated) adsorption mode is almost only half as stable as the η^2. For the couple ACPH/TFACPH, as for the couple AC/TFAC, the effect of fluorine is both to strengthen the η^2 bond to the surface (Fig. 8a) and to weaken the other possible adsorption modes (Figs. 8b and 8c). The resulting increased abundance of activated intermediate for TFACPH can explain the faster reaction rate observed for TFACPH in the racemic catalytic hydrogenation with respect to ACPH.

4. Conclusions

The theoretical study of the adsorption of activated ketones on platinum clusters indicates the following important features: (i) the rehybridization of the carbonyl carbon when the π system of the keto carbonyl lays on the metal; (ii) the activation of the C=O bond, evidenced by the extended stretching of the distance between the two atoms; (iii) the transformation of the originally prochiral ketone into a chiral surface species; (iv) the assisting effect of the ester in α position in stabilizing a hydrogen uptake in α-keto esters; and finally (v) the effect of fluorine in changing the relative proportion of differently adsorbed species, due to stabilization of the keto-carbonyl orbitals, that favors the presence of activated over spectator species on the surface.

On the basis of the calculations we are able to predict for ketones on platinum the existence of reaction intermediates that are to a large extent chemically different from the free molecules. The interaction with the metal results in the formation of different adsorbed species, of which one has features that resemble the corresponding alcohol, and others that resemble the free molecule. We call the species that resemble the alcohol *activated* toward the hydrogenation, while the others are spectator or precursor species for the same reaction. The hydrogenation rate can be enhanced by reduction of the activation barrier between the activated intermediate and the final product, due to a neighboring assisting functional group, which serves as hydrogen-bond acceptor for the incoming hydrogen, as seems to be the case for MP. On the other hand, the rate can be enhanced by the increase of the proportion between activated and spectator species, as may be the case for α-trifluorinated ketones. The adsorbed intermediate that we have termed activated toward hydrogenation can also be considered activated toward chiral discrimination because, differently from the original molecule, it contains a stereogenic carbon. The chiral-activated adsorbed intermediate is assumed to be able to discriminate the surrounding space during the interaction with the chiral modifier in a more efficient way than a prochiral intermediate would do.

Acknowledgments

Computing time has been provided by the ETH Zurich and by the Swiss Center for Scientific Computing (CSCS) in Manno. Financial support of the Swiss National Foundation is kindly acknowledged.

References

[1] A. Baiker, H.U. Blaser, in: G. Ertl, H. Knözinger, J. Weitkamp (Eds.), Handbook of Heterogeneous Catalysis, vol. 5, VCH, Weinheim, Germany, 1997, p. 2422.
[2] H.U. Blaser, H.P. Jalett, M. Müller, M. Studer, Catal. Today 37 (1997) 441.
[3] A. Baiker, J. Mol, Catal. A: Chem. 115 (1997) 473.
[4] P.B. Wells, A.G. Wilkinson, Top. Catal. 5 (1998) 39.
[5] A. Baiker, Curr. Opin. Solid State Mater. Sci. 3 (1998) 86.
[6] A. Baiker, J. Mol. Catal. A: Chem. 163 (2000) 205.
[7] A. Tai, T. Harada, in: Tailored Metal Catalysts, Reidel, Dordrecht, 1986, p. 265, and references therein.
[8] T. Osawa, T. Harada, O. Takayasu, Top. Catal. 13 (2000) 155.
[9] G.J. Hutchings, Chem. Commun. (1999) 301.
[10] G.V. Smith, F. Notheisz, Heterogeneous Catalysis in Organic Chemistry, Academic Press, San Diego, 1999.
[11] Y. Nitta, K. Kobiro, Chem. Lett. (1996) 897.
[12] K. Borszeky, T. Mallat, A. Baiker, Tetrahedron: Asym. 8 (1997) 3745.
[13] W.R. Huck, T. Mallat, A. Baiker, J. Catal. 193 (2000) 1.
[14] T. Mallat, M. Bodmer, A. Baiker, Catal. Lett. 44 (1997) 95.
[15] M. Bodmer, T. Mallat, A. Baiker, in: F.E. Herkes (Ed.), Catalysis in Organic Reactions, Dekker, New York, 1998, p. 75.
[16] A. Vargas, T. Bürgi, A. Baiker, New J. Chem. 26 (2002) 807.
[17] A. Vargas, T. Bürgi, M. von Arx, R. Hess, A. Baiker, J. Catal. 20 (2002) 489.
[18] ADF—Amsterdam Density Functional, Release 2002-01, Scientific Computing and Modelling NV, Vrije Universiteit, Theoretical Chemistry, Amsterdam.
[19] M. Saeys, M.-F. Reyniers, G.B. Marin, M. Neurock, J. Phys. Chem. 106 (2002) 7489.
[20] P.H.T. Philipsen, E. vanLenthe, J.G. Snijders, E.J. Baerends, Phys. Rev. B 56 (1997) 13556.
[21] G. Pacchioni, S.C. Chung, S. Kruger, N. Rosch, Surf. Sci. 392 (1997) 173.
[22] E. van Lenthe, E.J. Baerends, J.G. Snijders, J. Chem. Phys. 99 (1993) 4597;
E. van Lenthe, E.J. Baerends, J.G. Snijders, J. Chem. Phys. 101 (1994) 9783;
E. van Lenthe, E.J. Baerends, J.G. Snijders, J. Chem. Phys. 105 (1996) 6505;
E. van Lenthe, R. van Leeuwen, E.J. Baerends, J.G. Snijders, Int. J. Quantum Chem. 57 (1996) 281;
E. van Lenthe, E.J. Baerends, J.G. Snijders, J. Chem. Phys. 110 (1999) 8943.
[23] J.G. Snijders, E.J. Baerends, P. Ros, Mol. Phys. 38 (1979) 1909.
[24] G. te Velde, F.M. Bickelhaupt, E.J. Baerends, C. Fonseca Guerra, S.J.A. Van Gisbergen, J.G. Snijders, T. Ziegler, J. Comput. Chem. 22 (2001) 931.
[25] S.H. Vosko, L. Wilk, M. Nusair, Can. J. Phys. 58 (1980) 1200.
[26] A.D. Becke, Phys. Rev. A 38 (1988) 3098.
[27] J.P. Perdew, Phys. Rev. B 33 (1986) 8822.

[28] G.A. Somorjai, Introduction to Surface Chemistry and Catalysis, Wiley, New York, 1994.
[29] G. Schaftenaar, J.H. Noordik, J. Comput.-Aided Mol. Design 14 (2000) 123.
[30] M. von Arx, T. Mallat, A. Baiker, Tetrahedron: Asym. 12 (2001) 3089.
[31] M. von Arx, Doctoral thesis, Swiss Federal Institute of Technology, Zurich, No. 14322, 2001;
M. von Arx, T. Mallat, A. Baiker, in: D.C. Sherrington, A.P. Kybett (Eds.), Supported Catalysts and their Applications, Royal Society of Chemistry Special Publication, Cambridge, 2001, p. 247.
[32] N.R. Avery, W.H. Weinberg, A.B. Anton, B.H. Toby, Phys. Rev. Lett. 51 (1983) 682;
N.R. Avery, Surf. Sci. 125 (1983) 771;
A.B. Anton, N.R. Avery, B.H. Toby, W.H. Weinberg, J. Am. Chem. Soc. 108 (1986) 684.
[33] M. Neurock, V. Pallassana, in: D.G. Truhlar, K.Morokuma (Eds.), Transition State Modeling for Catalysis, in: ACS Symposium Series, vol. 721, 1999, p. 226, Chap. 18.
[34] M. Neurock, R.A. van Santen, J. Phys. Chem. B 104 (2000) 11127.
[35] K. Christmann, G. Ertl, T. Pignet, Surf. Sci. 54 (1976) 365.
[36] J. Horiuti, M. Polanyi, Trans. Faraday Soc. 30 (1934) 1164.
[37] Y. Orito, S. Imai, S. Niwa, Collected papers of the 43rd Catalysis Forum, Japan, 1978, p. 30;
Y. Orito, S. Imai, S. Niwa, G.H. Nguyen, J. Synth. Org. Chem. Jpn. 37 (1979) 173;
Y. Orito, S. Imai, S. Niwa, J. Chem. Soc. Jpn. (1979) 1118, (1980) 670, (1982) 137.
[38] M. Castonguay, J.R. Roy, A. Rochefort, P.H. McBreen, J. Am. Chem. Soc. 122 (2000) 518.
[39] T. Bürgi, F. Atamny, A. Knop-Gericke, M. Hävecker, T. Schedel-Niedrig, R. Schlögl, A. Baiker, Catal. Lett. 66 (2000) 109.
[40] T. Bürgi, F. Atamny, R. Schlögl, A. Baiker, J. Phys. Chem. B 104 (2000) 5953.
[41] J.M. Bonello, F.J. Williams, A.K. Santra, R.M. Lambert, J. Phys. Chem. B 104 (2000) 9696.
[42] S.F. Boys, F. Bernardi, Mol. Phys. 19 (1970) 553.
[43] W.A.H. Vermeer, A. Fulford, P. Johnston, P.B. Wells, Chem. Commun. (1993) 1053.
[44] M. Studer, V. Okafor, H.U. Blaser, Chem. Commun. (1998) 1053.
[45] E. Toukoniitty, P. Mäki-Arvela, M. Kuzma, A. Villela, A.K. Neyestanaki, T. Salmi, R. Sjöholm, R. Leino, E. Laine, D.J. Murzin, J. Catal. 204 (2001) 281.
[46] O.J. Sonderegger, T. Bürgi, A. Baiker, J. Catal. 215 (2003) 116.
[47] B. Török, K. Felföldi, K. Balázsik, M. Bartók, Chem. Commun. (1999) 1725.
[48] M. Studer, S. Burkhardt, H.U. Blaser, Chem. Commun. (1999) 1727.
[49] M. Studer, H.U. Blaser, S. Burkhardt, Adv. Synth. Catal. 344 (2002) 511.
[50] P.R.N. de Souza, D.A.G. Aranda, J.W. de M.Carneiro, C.da S.B. de Oliveira, O.A.C. Antunes, F.B. Passos, Int. J. Quantum Chem. 92 (2003) 400.
[51] C. Xu, Y.L. Tsai, B.E. Koel, J. Phys. Chem. 98 (1994) 585.
[52] J.M. Campbell, S.G. Seimanides, C.T. Campbell, J. Phys. Chem. 93 (1989) 815.